I. ADDITIONAL INFORMATION ON DIRECTIONAL TRANSPORT

This section aims to provide additional information about the directional emission experiments presented in the main paper. In these experiments, the two pump spots are located in two adjacent sites, with photon frequencies corresponding the central energy of the band dispersion. To quantify the directional emission in the lattice, we define the total intensities emitted to the left and right of the pumped region as

$$I_L = \sum_{m<m_{\text{pump}}} I_m; \quad I_R = \sum_{m>m_{\text{pump}}} I_m,$$

where I_m denotes the intensity at lattice site m after normalisation of the total emitted intensity in all lattice sites to 1: $I_{total} = \sum_m I_m = 1$. The pump lattice sites are denote and m_{pump} (in our case, sites 19 and 20). The pumped sites are excluded from the summation to ensure that only the transported intensity is considered.
The directional transport (D) is then defined as

$$D = \frac{I_R - I_L}{I_R + I_L}.$$

By definition, D lies in the range $[-1, 1]$ and provides the fraction of directional emission. $D = 0$ implies symmetric emission to both sides. Positive values of D indicate net rightward transport, while negative values indicate leftward transport. Figure 1(a) presents the directional transport D as a function of the phase difference $\Delta\phi/\pi$ between the two laser spots obtained from simulations of Eqs. (3) and (4) of the main text. Figure 1(b) shows the corresponding experimental results.

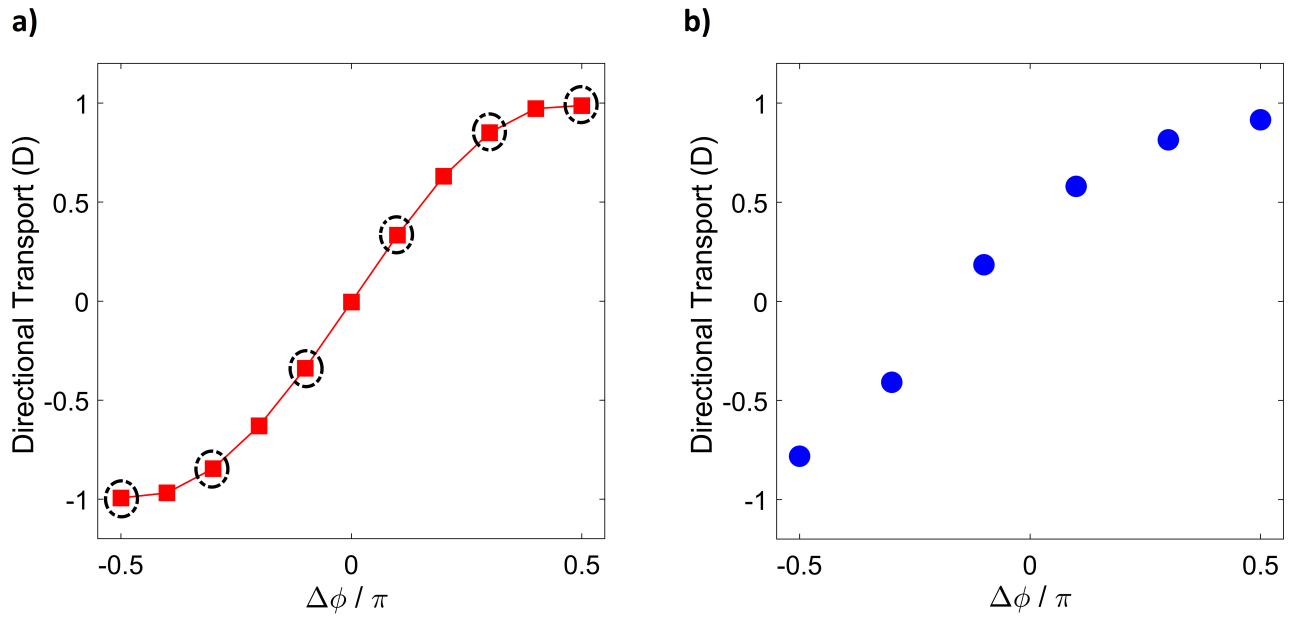

FIG. 1. Phase dependent directional transport $D(\Delta\phi)$ extracted from both numerical simulations 1(a) and experimental measurements 1(b). The six black circles in Fig. 1(a) mark the phase values used in the experimental measurements shown along the x-axis in Fig. 1(b).

To gain further insights on the transition from the left to right directional transport, we compare the spatial intensity profiles measured experimentally and numerically as a function of the phase difference between the two pump spots. As shown in Figs. 2 and 3, tuning the phase difference from -0.5π to $+0.5\pi$ induces a gradual shift in the direction of light propagation within the lattice. This behavior arises from constructive and destructive interference between drive and lattice eigenmodes, which alters the balance between left- and right- propagating components. Both simulations and experiments exhibit the strongest asymmetry at $\Delta\phi = \pm\frac{\pi}{2}$: a phase difference of $-\pi/2$ leads to maximum transport to the left, while $+\pi/2$ results in maximum transport to the right.

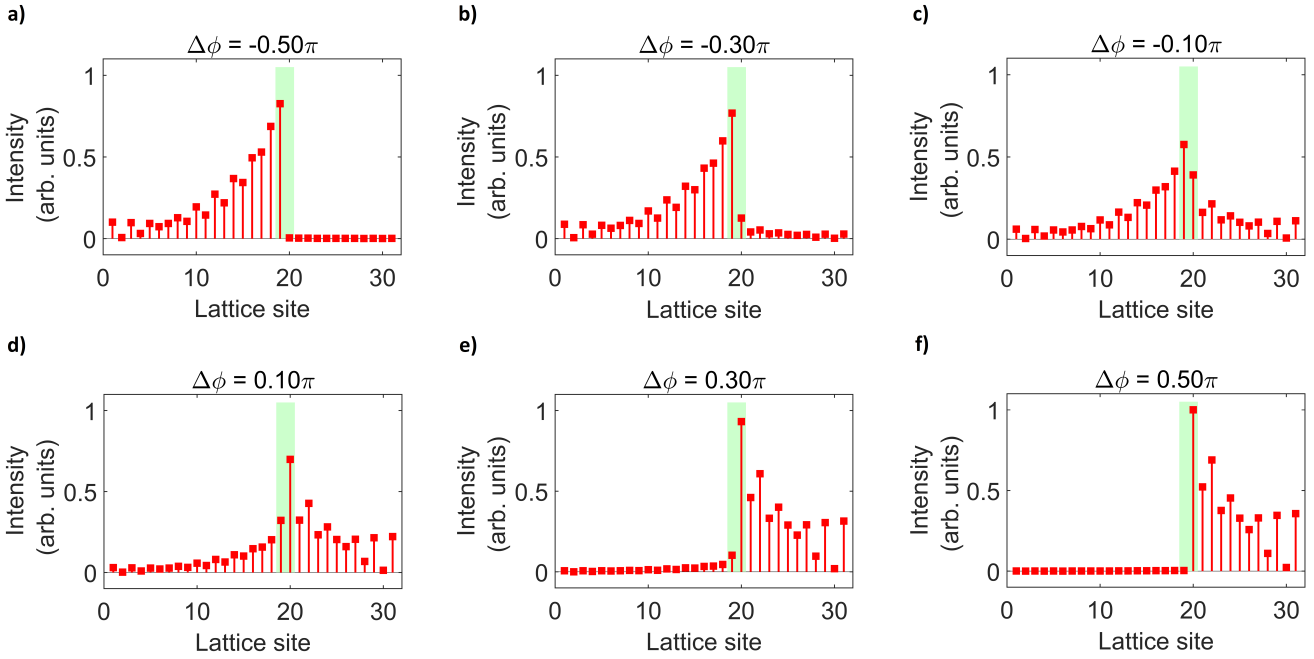

FIG. 2. (a–f) Numerical steady-state intensity profiles for different pump phase differences $\Delta\phi$ between two adjacent sites, ranging from -0.5π to 0.5π. The laser detuning $\Delta/t = 0$. The strongest leftward transport occurs at $\Delta\phi = -0.5\pi$, and rightward transport is maximized at $\Delta\phi = +0.5\pi$. Shaded areas correspond to the sites $(19, 20)$ where the external pump is applied.

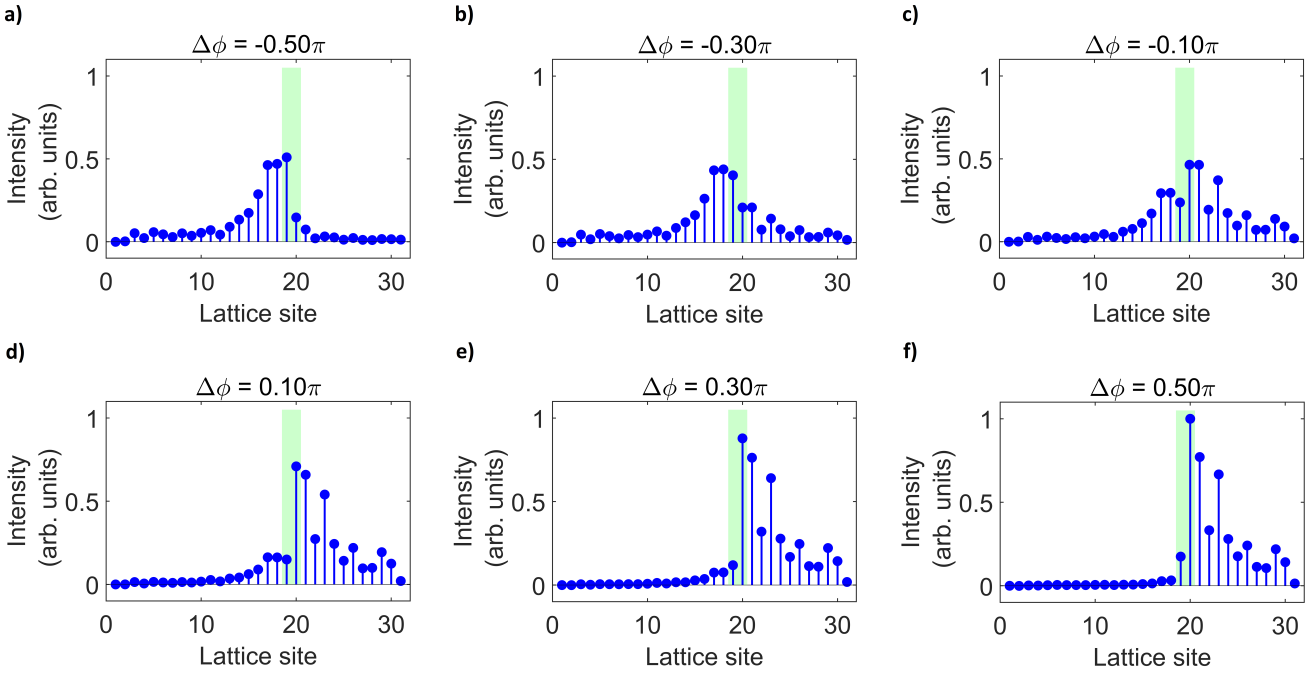

FIG. 3. (a–f) Experimentally measured intensity profiles for different pump phase differences $\Delta\phi$ between two adjacent sites, ranging from -0.5π to 0.5π. Each panel corresponds to a distinct phase difference between the two excitation spots showing qualitative agreement with the numerical results in Fig. 2. Shaded areas correspond to the sites $(19, 20)$ where the external pump is applied.

II. ANALYTICAL DERIVATION OF SITE INTENSITY

This section aims to provide an analytical description the spatial light distribution within photonic lattices in the linear regime. To simplify the calculation without losing important features, we assume a polariton to be 100% photonic (and thus having no interaction) and we neglect the contribution originating from next-nearest neighbor coupling ($t' = 0$). Under these assumptions, we can write a driven-dissipative tight-binding model, in the rotating frame of the pump laser, describing the dynamics of the photon field ψ_m on each site m:

$$i\hbar\dot{\psi}_m = (\epsilon_0 - \omega_p)\psi_m - i\gamma\psi_m - t(\psi_{m+1} + \psi_{m-1}) + F_m, \tag{1}$$

where ϵ_0 is the middle band photonic energy, γ is the radiative decay, t is the nearest neighbor coupling and F_m is the field source term.

It is convenient to write the problem in the reciprocal space using $\psi_m = \frac{1}{\sqrt{M}}\sum_k \psi_k e^{ikm}$ and $F_m = \frac{1}{\sqrt{M}}\sum_k F_k e^{ikm}$ to get:

$$i\hbar\dot{\psi}_k = (\epsilon_0 - \omega_p)\,\psi_k - i\gamma\psi_k - 2t\cos k\,\psi_k + F_k,$$

with $k \in [-\pi, \pi]$ and M the total number of sites. Introducing $\Delta = \omega_p - \epsilon_0$ and looking for a steady state solution, we obtain

$$\psi_k = \frac{F_k}{\Delta + 2t\cos k + i\gamma}.$$

We focus on the situation of interest in the main section of the paper, where only two sites m_1 and m_2 are pumped with a phase difference of $\Delta\phi$. Such pumping can be explicitly written in position space like:

$$F_m = \frac{F}{\sqrt{M}}(\delta_{m,m_1} + e^{i\Delta\phi}\delta_{m,m_2}),$$

with $\delta_{m,n}$ the Kronecker delta, or in Fourier space as:

$$F_k = \sum_m F_m e^{-ikm} = \frac{F}{\sqrt{M}}\left(e^{-ikm_1} + e^{i\Delta\phi}e^{-ikm_2}\right).$$

We can write the momentum space components of the steady-state solution:

$$\psi_k = \frac{F}{\sqrt{M}}\frac{e^{-km_1} + e^{i\Delta\phi}e^{-ikm_2}}{\Delta + 2t\cos k + i\gamma}.$$

We transform back to real space and approximate the discrete sum in momenta by an integral to obtain

$$\psi_m = \frac{1}{\sqrt{M}}\sum_k \psi_k e^{ikm} \approx \frac{F}{2\pi}\int_{-\infty}^{\infty}\frac{e^{ik(m-m_1)} + e^{i\Delta\phi}e^{ik(m-m_2)}}{\Delta + 2t\cos k + i\gamma}dk, \tag{2}$$

where the integration limits have been extended from $-\infty$ to ∞ because the integrand vanishes outside the first Brillouin zone. This integral can be calculated using complex analysis and the residue theorem. Depending on the sign of $m - m_1$ and $m - m_2$, the exponential terms $e^{ik(m-m_j)}$ determine whether the integration contour should be closed in the upper or lower half of the complex k-plane. The three scenarios for this are:

1. The considered site is to the left of the two pumped sites: $m < m_1 < m_2 \Rightarrow m - m_1 < 0$ and $m - m_2 < 0$
2. The considered site is in between the two pumped sites: $m_1 < m < m_2 \Rightarrow m - m_1 > 0$ and $m - m_2 < 0$
3. The considered site is to the right of the two pumped sites: $m_1 < m_2 < m \Rightarrow m - m_1 > 0$ and $m - m_2 > 0$

Following the derivation as shown in Appendix B of Ref. [1], we will investigate the above three scenarios and conduct the calculation explicitly in one of them to show that we obtain the expression presented in the main paper (Eq. (5) of the main text). The calculations in the other two scenarios are similar and present no additional complexities compared to the presented one.

Case 1: $m - m_1 < 0$ **and** $m - m_2 < 0$

In this case, Eq. (2) can be written in the following way, with explicit negative signs in the complex exponent in the integrands:

$$\psi_m \approx \frac{F}{2\pi} \int_{-\infty}^{\infty} \frac{e^{-ik|m-m_1|} + e^{i\Delta\phi} e^{-ik|m-m_2|}}{\Delta + 2t\cos k + i\gamma} dk.$$

To evaluate the above integral using the residue theorem, we identify the poles of the integrand in the complex k-plane. These occur where the denominator vanishes and therefore the dominant contribution arises from the poles closest to the real axis:

$$\Delta + 2t\cos k \approx 0.$$

Here, we define the resonant momentum k_0 through:

$$\cos k_0 = -\frac{\Delta}{2t} \quad \Rightarrow \quad k_0 = \arccos\left(-\frac{\Delta}{2t}\right).$$

Then, we expand $\cos k$ around $k = k_0$ up to first-order in k to get

$$\cos k \approx \cos k_0 - \sin k_0 (k - k_0).$$

Performing some algebra by multiplying both sides by $2t$, substituting $\cos k_0$ by $-\frac{\Delta}{2t}$ and re-arranging the expression, we obtain:

$$\Delta + 2t\cos k \approx -2t\sin k_0 (k - k_0).$$

Identifying $\sin k_0$ as:

$$\sin k_0 = \sqrt{1 - \cos^2 k_0} = \sqrt{1 - \left(\frac{\Delta}{2t}\right)^2} = \frac{\sqrt{4t^2 - \Delta^2}}{2t},$$

and plugging in the previous expression, we finally get:

$$\Delta + 2t\cos k \approx -\sqrt{4t^2 - \Delta^2}(k - k_0)$$

Doing the same calculation for $k \approx -k_0$, we get:

$$\Delta + 2t\cos k \approx +\sqrt{4t^2 - \Delta^2}(k + k_0),$$

Finally, we have

$$\Delta + 2t\cos k \approx \begin{cases} -\sqrt{4t^2 - \Delta^2}\ \left[k - \arccos\left(\frac{-\Delta}{2t}\right)\right] & \text{for } k \text{ close to } k_0 \\ +\sqrt{4t^2 - \Delta^2}\ \left[k + \arccos\left(\frac{-\Delta}{2t}\right)\right] & \text{for } k \text{ close to } -k_0 \end{cases}$$

where

$$k_0 \equiv \arccos\left(\frac{-\Delta}{2t}\right),$$

These expressions allow us to transform Eq. (2) into the following integral in which the integrand is only important around the two poles at k_0 and $-k_0$:

$$\psi_m \approx \frac{F}{2\pi} \int_{-\infty}^{\infty} \left[\frac{e^{-ik|m-m_1|} + e^{i\Delta\phi} e^{-ik|m-m_2|}}{-\sqrt{4t^2 - \Delta^2}(k - k_0) + i\gamma} + \frac{e^{-ik|m-m_1|} + e^{i\Delta\phi} e^{-ik|m-m_2|}}{+\sqrt{4t^2 - \Delta^2}(k + k_0) + i\gamma} \right] dk \tag{3}$$

At this stage, it is informative to compute the density of state (DOS) to understand how it appears in the final expression. Indeed, the density of states (DOS) is defined by:

$$D(E) = \left|\frac{dk}{dE}\right| = \left|\frac{1}{\frac{dE}{dk}}\right|.$$

Starting from the dispersion relation given by:

$$E(k) = -2t\cos k \Rightarrow \frac{dE}{dk} = 2t\sin k \Rightarrow D(E) = \left|\frac{1}{2t\sin k}\right|$$

and substituting $\cos k_0 = -\frac{\Delta}{2t}$, we get:

$$\sin k_0 = \sqrt{1-\cos^2 k_0} = \frac{\sqrt{4t^2-\Delta^2}}{2t}$$

which brings

$$D(\Delta) = \frac{1}{\sqrt{4t^2-\Delta^2}}.$$

Substituting $D(\Delta)$ in Eqn. (3), we obtain

$$\psi_m \approx -\frac{FD(\Delta)}{2\pi}\int_{-\infty}^{+\infty}\left\{\underbrace{\frac{e^{-ik|m-m_1|}}{k-k_0-i\gamma D(\Delta)}}_{(1)} + \underbrace{e^{i\Delta\phi}\frac{e^{-ik|m-m_2|}}{k-k_0-i\gamma D(\Delta)}}_{(2)} - \underbrace{\frac{e^{-ik|m-m_1|}}{k+k_0+i\gamma D(\Delta)}}_{(3)} - \underbrace{e^{i\Delta\phi}\frac{e^{-ik|m-m_2|}}{k+k_0+i\gamma D(\Delta)}}_{(4)}\right\}dk$$

We can now evaluate individual integrals using the residue theorem to get an expression for $|\psi_m|^2$.

The integrand term (1) has a pole at $k = k_0 + i\gamma D(\Delta)$, which lies in the upper-half complex plane. Since $|m-m_1| > 0$, the exponential $e^{-ik|m-m_1|}$ decays as $\mathrm{Im}(k) \to -\infty$, i.e., in the lower-half plane. To ensure convergence, the contour is closed in the lower-half, which does not enclose the pole. Therefore, the integral is zero.

$$\int_{-\infty}^{+\infty} dk \frac{e^{-ik|m-m_1|}}{k-k_0-i\gamma D(\Delta)} = 0$$

Similar to the first term, the integrand term (2) has a pole at $k = k_0 + i\gamma D(\Delta)$ that lies in the upper-half plane. The exponential $e^{-ik|m-m_2|}$ decays in the lower-half, so the contour is again closed downward and the pole is not enclosed. Thus, the integral evaluates to zero.

$$\int_{-\infty}^{+\infty} dk \frac{e^{-ik|m-m_2|}}{k-k_0-i\gamma D(\Delta)} = 0$$

The integrand term (3) has a pole at $k = -k_0 - i\gamma D(\Delta)$, which lies in the lower-half plane. Since $|m-m_1| > 0$, the exponential $e^{-ik|m-m_1|}$ also decays in the lower-half. Therefore, we close the contour in the lower-half, and the pole is enclosed. The residue contributes, yielding a non-zero result ($e^{-i(-k_0-i\gamma D(\Delta))|m-m_1|} = e^{+ik_0|m-m_1|}e^{-\gamma D(\Delta)|m-m_1|}$), which brings

$$\int_{-\infty}^{+\infty} dk \frac{e^{-ik|m-m_1|}}{k+k_0+i\gamma D(\Delta)} = -2\pi i\, e^{+ik_0|m-m_1|}\, e^{-\gamma D(\Delta)|m-m_1|}$$

The integrand term (4) follows the same logic as the third: it has a pole at $k = -k_0 - i\gamma D(\Delta)$ which lies in the lower-half plane, and the exponential decays there as well. Thus, closing the contour downward encloses the pole, and the residue contributes a non-zero value.

$$\int_{-\infty}^{+\infty} dk \frac{e^{-ik|m-m_2|}}{k+k_0+i\gamma D(\Delta)} = -2\pi i\, e^{+ik_0|m-m_2|}\, e^{-\gamma D(\Delta)|m-m_2|}$$

Thus, assembling all these results together we obtain the follwoing expression for the field at sites located at the left of the pumping spots:

$$\psi_m = -FD(\Delta)i\left[e^{ik_0|m-m_1|}e^{-\gamma D(\Delta)|m-m_1|} + e^{i\Delta\phi}e^{ik_0|m-m_2|}e^{-\gamma D(\Delta)|m-m_2|}\right]$$

Taking the square modulus brings:

$$I_m = |\psi_m|^2 = |F|^2 D(\Delta)^2 \left|e^{ik_0|m-m_1|}e^{-\gamma D(\Delta)|m-m_1|} + e^{i\Delta\phi}e^{ik_0|m-m_2|}e^{-\gamma D(\Delta)|m-m_2|}\right|^2$$

We recover the equation present in the main text. In the following, we show the different cases for completeness, but we do not reproduce all the details of the calculations. We mainly explain how we recover the same expression for I_m.

Case 2: $m - m_1 > 0$ **and** $m - m_2 < 0$

Using the same derivation as in case 1, and taking care of the right sign of the complex exponents in case (2), we obtain an equation similar to Eq. (3):

$$\psi_m \approx -\frac{FD(\Delta)}{2\pi}\int_{-\infty}^{+\infty}\left\{\underbrace{\frac{e^{ik|m-m_1|}}{k-k_0-i\gamma D(\Delta)}}_{(1)} + \underbrace{\frac{e^{i\Delta\phi}e^{-ik|m-m_2|}}{k-k_0-i\gamma D(\Delta)}}_{(2)} - \underbrace{\frac{e^{ik|m-m_1|}}{k+k_0+i\gamma D(\Delta)}}_{(3)} - \underbrace{\frac{e^{i\Delta\phi}e^{-ik|m-m_2|}}{k+k_0+i\gamma D(\Delta)}}_{(4)}\right\}dk$$

This case is symmetric to case 1, but the roles of m_1 and m_2 are reversed in terms of which exponential contributes. Terms (1) and (4) now contribute to the integral, while (2) and (3) vanish. The derivation proceeds in exactly the same manner, and the resulting expression for I_m is unchanged.

Case 3: $m - m_1 > 0$ **and** $m - m_2 > 0$

Similarly, we get the following expression:

$$\psi_m \approx -\frac{FD(\Delta)}{2\pi}\int_{-\infty}^{+\infty}\left\{\underbrace{\frac{e^{ik|m-m_1|}}{k-k_0-i\gamma D(\Delta)}}_{(1)} + \underbrace{\frac{e^{i\Delta\phi}e^{ik|m-m_2|}}{k-k_0-i\gamma D(\Delta)}}_{(2)} - \underbrace{\frac{e^{ik|m-m_1|}}{k+k_0+i\gamma D(\Delta)}}_{(3)} - \underbrace{\frac{e^{i\Delta\phi}e^{ik|m-m_2|}}{k+k_0+i\gamma D(\Delta)}}_{(4)}\right\}dk$$

In this case, both exponential terms $e^{ik|m-m_1|}$ and $e^{ik|m-m_2|}$ decay in the upper-half complex plane. As a result, the contour is closed in the upper-half, enclosing the poles at $k = k_0 + i\gamma D(\Delta)$. The poles of the first two terms lie in the upper-half plane and are enclosed. Therefore, only the contributions from terms (1) and (2) yield non-zero residues. After applying the residue theorem, we again obtain the same structure for ψ_m, and consequently the same final expression for the intensity $I_m = |\psi_m|^2$.

Therefore, in all three cases, we get the following result;

$$I_m = |\psi_m|^2 = |F|^2 D(\Delta)^2 \left|e^{ik_0|m-m_1|}e^{-\gamma D(\Delta)|m-m_1|} + e^{i\Delta\phi}e^{ik_0|m-m_2|}e^{-\gamma D(\Delta)|m-m_2|}\right|^2 \tag{4}$$

A. Derivation of the criteria for directionality

To derive the conditions under which directional emission occurs, we analyze the steady-state intensity in the region to the left of both pump sites, i.e., for $m < m_1$ and $m < m_2$, that is, case 1. The link with the general expression

is made by having in mind that $(m-m_1) = -|m-m_1|$ and $(m-m_2) = -|m-m_2|$. Identifying the conditions for complete destructive interference, we can determine the values of $\Delta\phi$ and k_0 that suppress propagation in this direction and thus lead to directional transport. Specifically, the intensity at the site m takes the form:

$$I_m = |F|^2 D(\Delta)^2 \underbrace{\left| e^{-ik_0(m-m_1)} e^{\gamma D(\Delta)(m-m_1)} + e^{i\Delta\phi} e^{-ik_0(m-m_2)} e^{\gamma D(\Delta)(m-m_2)} \right|^2}_{0 \text{ (complete destructive interference)}}$$

$$I_m = |F|^2 D(\Delta)^2 |A+B|^2 = |F|^2 D(\Delta)^2 (|A|^2 + |B|^2 + A^*B + AB^*)$$

$$\begin{aligned} A &= e^{-ik_0(m-m_1)} e^{\gamma D(\Delta)(m-m_1)} \\ B &= e^{i\Delta\phi} e^{-ik_0(m-m_2)} e^{\gamma D(\Delta)(m-m_2)} \end{aligned}$$

$$\begin{aligned} |A|^2 &= e^{2\gamma D(\Delta)(m-m_1)} \\ |B|^2 &= e^{2\gamma D(\Delta)(m-m_2)} \\ A^*B &= e^{i\Delta\phi} e^{ik_0(m_2-m_1)} e^{\gamma D(\Delta)(2m-m_1-m_2)} \\ AB^* &= e^{-i\Delta\phi} e^{-ik_0(m_2-m_1)} e^{\gamma D(\Delta)(2m-m_1-m_2)} \end{aligned}$$

Therefore,

$$I_m/(|F|^2 D(\Delta)^2) = e^{2\gamma D(\Delta)(m-m_1)} + e^{2\gamma D(\Delta)(m-m_2)} + e^{\gamma D(\Delta)(2m-m_1-m_2)} \left[2\cos\left(\Delta\phi + k_0(m_2-m_1)\right)\right].$$

In the limit of small γ compared to $t|m_1-m_2|$, we have $e^{-\gamma D(\Delta)|m-m_2|} \approx e^{-\gamma D(\Delta)|m-m_1|}$ allowing us to write

$$I_m/(|F|^2 D(\Delta)^2) \approx 2e^{2\gamma D(\Delta)(m-m_1)} \left[1 + \cos\left(\Delta\phi + k_0(m_2-m_1)\right)\right],$$

which is equal to 0 in the case where

$$\Delta\phi + k_0(m_2-m_1) = (2\ell+1)\pi, \quad \ell \in \mathbb{Z}.$$

B. Derivation of the criteria for linear localization

To analytically investigate the conditions under which localization arises in Eqn. (4), we consider the steady-state field amplitude at an arbitrary site m resulting from coherent driving at two sites m_1 and m_2. In the limit of small γ compared to $t|m_1-m_2|$, we have $e^{-\gamma D(\Delta)|m-m_2|} \approx e^{-\gamma D(\Delta)|m-m_1|}$, allowing us to write the field as

$$\psi_m = FD(\Delta) e^{-\gamma D(\Delta)|m-m_2|} \left[e^{ik_0|m-m_1|} + e^{i\Delta\phi} e^{ik_0|m-m_2|} \right]. \tag{5}$$

We want to identify how constructive or destructive interference between the two driving fields can lead to enhanced localization at specific sites, depending on the pump separation and relative phase. We aim to find conditions on $\Delta\phi$ and k_0 such that:

1. Destructive interference occurs at all sites $m \leq m_1$,

2. Destructive interference occurs at all sites $m \geq m_2$,

1. Destructive Interference for $m \leq m_1$

Introducing $p \geq 0$ such that $m = m_1 - p$ we have:

$$|m - m_1| = p, \quad |m - m_2| = d + p, \quad \text{where } d = m_2 - m_1$$

$$\psi_m = FD(\Delta) e^{-\gamma D(\Delta)|m-m_2|} e^{ik_0 p} \left(1 + e^{i(\Delta\phi + k_0 d)}\right)$$

Destructive interference conditions requires $\psi_m = 0$ which is satisfied for:

$$\boxed{1 + e^{i(\Delta\phi + k_0 d)} = 0} \tag{6}$$

2. Destructive Interference for $m \geq m_2$

Introducing $p_2 \geq 0$ such that $m = m_2 + p_2$ we have:

$$|m - m_1| = d + p_2, \quad |m - m_2| = p_2$$

$$\psi_m = FD(\Delta) e^{-\gamma D(\Delta)|m-m_2|} e^{ik_0 (d+p_2)} \left(1 + e^{i(\Delta\phi - k_0 d)}\right)$$

Destructive interference conditions requires $\psi_m = 0$ which is satisfied for:

$$\boxed{1 + e^{i(\Delta\phi - k_0 d)} = 0} \tag{7}$$

Assembling these conditions of Eqn. (6) and (7) require simultaneously satisfying:

$$\Delta\phi = (2n+1)\pi + k_0 d \tag{i}$$
$$\Delta\phi = (2n+1)\pi - k_0 d, \tag{ii}$$

As $\Delta\phi$ is defined modulo 2π, the only solution is $k_0 d = \pm\pi$. Knowing that $d = 2$, it follows that k_0 has to be equal to $\pm\frac{\pi}{2}$. These k_0 values are satisfied only for a detuning $\Delta = 0$, providing the condition to observe localization.

III. EFFECT OF DISORDER IN NUMERICAL SIMULATION

To study the effects of disorder in the localization of light when the pump spots are separated by two sites (m and $m+2$) we do numerical simulations including disorder in either onsite energy of hopping energy. For each value of disorder strength α, the system was simulated with 25 independent disorder realizations. At each realization, the steady-state intensity profile was extracted and normalized. The resulting spatial profiles were then averaged to obtain the disorder-averaged intensity distribution. The error bars represent the standard deviation of the intensity at each site across these 25 realizations, indicating the spread due to random disorder. For the simulations presented in Fig. 4 and 5 below, the pump spots are located at lattice sites 15 and 17, with a laser detuning of $\Delta/t = -0.21$, with $t = 0.35$meV (nearest-neighbor hopping) and $t' = -0.03$meV (next-nearest-neighbor hopping).

A. Onsite Disorder

The on-site disorder for $i \in \{\text{photon}, \text{exciton}\}$ is given by:

$$\text{onsite\_disorder}_i = \alpha \cdot t \cdot [\text{rand}(1, N_{\text{pillars}}) - 0.5]$$

where α is the disorder strength, t is the unperturbed nearest hopping energy and $\text{rand}(1, N_{\text{pillars}})$ generates a random array of values uniformly distributed in the interval $[0, 1]$. The subtraction of 0.5 centers the disorder around zero.

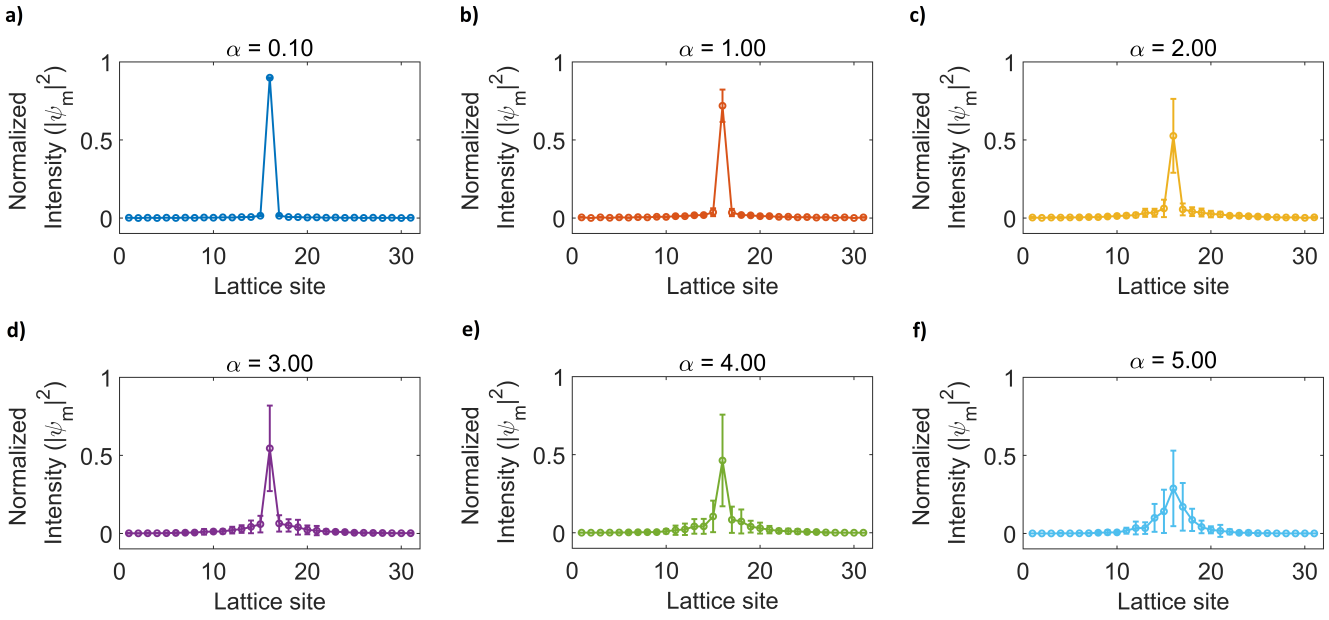

FIG. 4. Normalized intensity profiles for increasing onsite disorder strength α. (a)–(f) correspond to: (a) $\alpha = 0.1$, (b) $\alpha = 1$,(c) $\alpha = 2$, (d) $\alpha = 3$, (e) $\alpha = 4$ and (f) $\alpha = 5$.

B. Hopping Disorder

The hopping disorder for the nearest-neighbor (t) and next-nearest-neighbor (t') couplings is introduced as:

$$t_{\text{disorder}} = t + \alpha \cdot t \cdot [\text{rand}(1, N_{\text{pillars}} - 1) - 0.5]$$
$$t'_{\text{disorder}} = t' + \alpha \cdot t' \cdot [\text{rand}(1, N_{\text{pillars}} - 2) - 0.5]$$

where t, t' are the unperturbed hopping amplitudes, α is the disorder strength (same as for the on-site disorder), $\text{rand}(1, N)$ generates a uniformly distributed random array in $[0, 1]$.

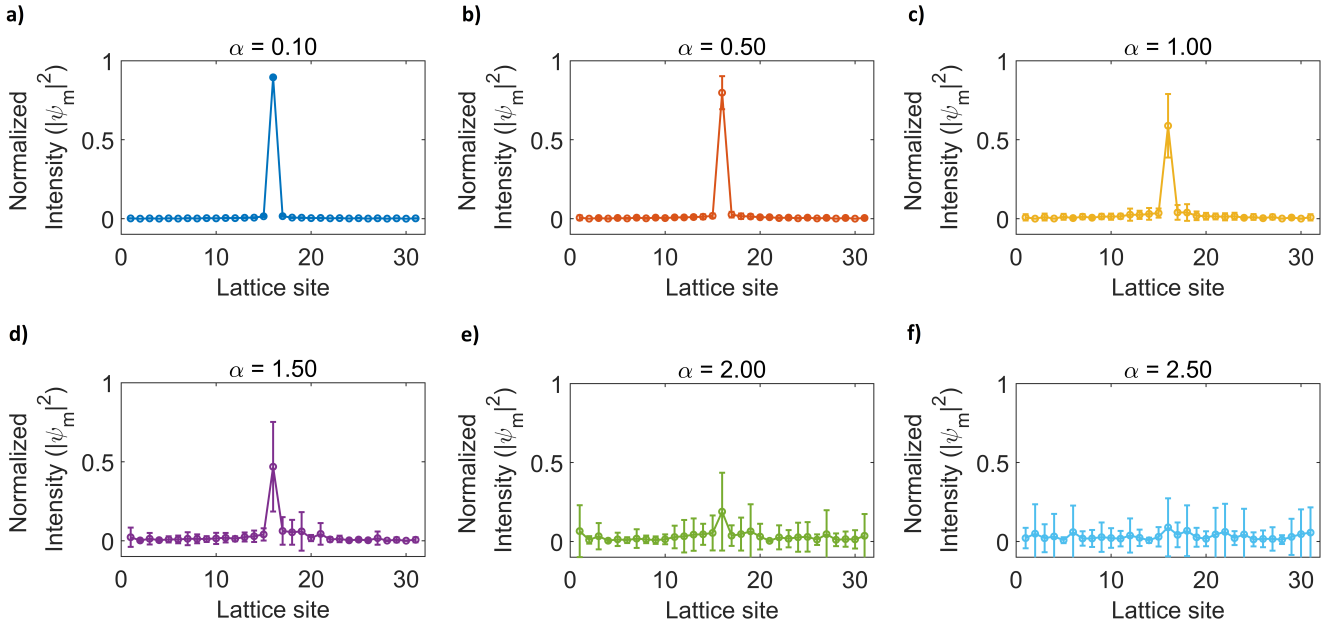

FIG. 5. Normalized intensity profiles for increasing hopping disorder strength α. (a)–(f) correspond to: (a) $\alpha = 0.1$, (b) $\alpha = 0.5$,(c) $\alpha = 1$, (d) $\alpha = 1.5$, (e) $\alpha = 2$ and (f) $\alpha = 2.5$.

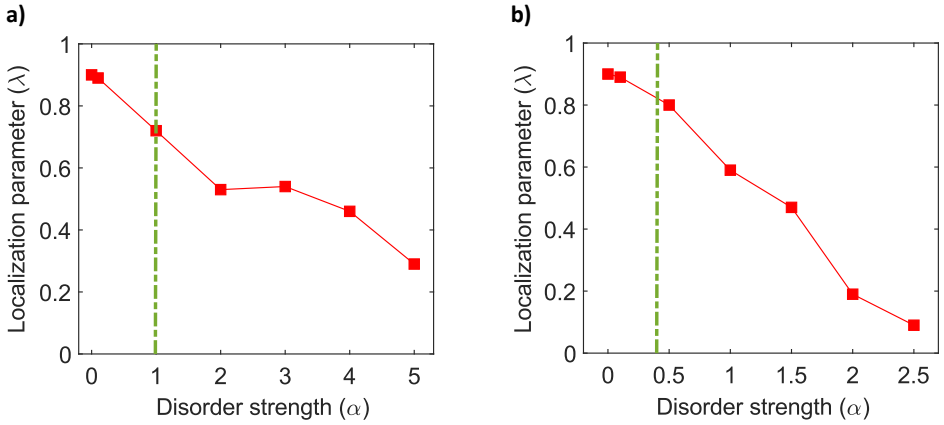

FIG. 6. Disorder-averaged localization parameter (λ) as a function of disorder strength (α). (a) Onsite disorder, (b) Hopping disorder.

Figures 6(a) and 6(b) show the localization parameter as a function of disorder strength for onsite and hopping disorder, respectively, extracted from the numerical data displayed in Figs. 4 and 5. A vertical green line is included in each panel to indicate the maximum allowable disorder strength that still preserves good agreement with the experimental dispersion. For disorder values below the green line, the localization parameter is higher than the measured one, suggesting that disorder might not be the main reason for the deviation between the measured localization parameter and the simulated one from Eqs. (3) and (4) of the main text.

IV. EFFECT OF STRAY LIGHT IN NUMERICAL SIMULATION

A. Linear Regime

To understand why the localization parameter (λ) appears lower in the experimental data compared to numerical simulations, we investigated the effect of stray light. We focus on the case with detuning $\Delta/t = -0.21$, where localization reaches its maximum in the linear regime, with two pump spots applied at lattice sites 15 and 17. For this detuning, the intensity at the maximally localized site (site 16) in the numerics was matched to the corresponding experimental intensity, as shown in Fig. 7(a).

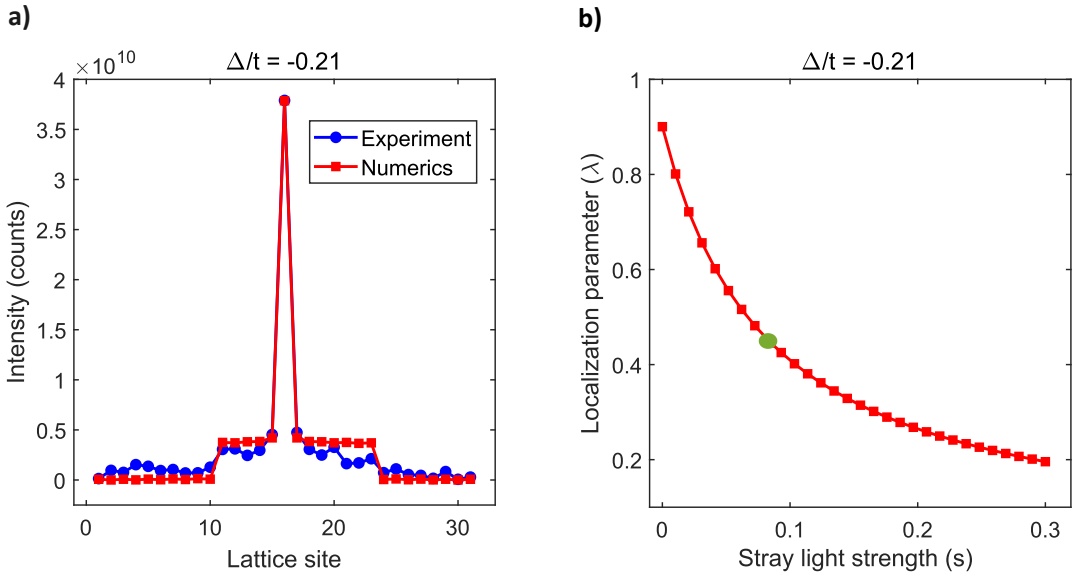

FIG. 7. (a) Intensity profile (with stray light strength $s = 0.085$) compared to the experimental data at $\Delta/t = -0.21$. (b) Localization parameter λ as a function of stray light strength s.

Stray light was added as a static background intensity individually to the affected sites (11-15 and 17-23), and the stray light strength s was determined by tuning its value such that the simulated real-space intensity profile approximately reproduces the experimental intensity at the affected sites. This procedure yields a stray light strength of $s = 0.085$, corresponding to 8.5% per site in the region 11-15 and 17-23 of the total lattice intensity at steady state. The method for incorporating stray light and computing the localization parameter λ is as follows. Let I_n denote the steady-state intensity at site n, obtained from solving the two coupled equations (3) and (4) of the main text. The stray light contribution is defined as

$$I_n^{\text{stray}} = \begin{cases} s \sum_{m=1}^{N} I_m, & \text{if } n \in S, \\ 0, & \text{otherwise,} \end{cases} \tag{6}$$

where $S \subset \{1, \ldots, N\}$ is the set of stray light affected sites. The total intensity is then

$$I_n^{\text{total}} = I_n + I_n^{\text{stray}} \tag{7}$$

and the localization parameter is calculated as

$$\lambda = \frac{I_{16}}{\sum_{n=1}^{N} I_n^{\text{total}}} \tag{8}$$

where I_{16} is the intensity at the maximum localized site (in between the two pump spots). This approach enables us to quantitatively assess how the presence of stray light reduces the localization parameter (λ) in the experiment.

In Fig. 7(a), the intensity profile obtained from the numerics (with stray light included at $s = 0.085$) against the experimentally measured profile at $\Delta/t = -0.21$ is plotted. Figure 7(b) shows the computed localization parameter λ as a function of stray light strength s. As expected, λ decreases with increasing s, reflecting the delocalizing effect of stray light. The localization parameter corresponding to $s = 0.085$ is highlighted with a green circle which corresponds to $\lambda = 0.445$, matching the experiment value of 0.44.

B. Non-Linear Regime

From the stray light strength identified from the green circle ($s = 0.085$) in Fig. 7(b), we investigate the effect of stray light in the non-linear regime by numerically calculating the localization parameter (λ) as a function of pump power. Figure 8 presents two cases at $\Delta/t = -0.21$: one without stray light and the other with stray light included. In the absence of stray light, λ decreases significantly from 0.90 to 0.38 as the pump power increases, indicating strong nonlinear delocalization as power increases for this specific detuning. In contrast, when stray light is present, λ decreases more gradually, from 0.445 to 0.32. This slower drop suggests that the presence of background intensity (stray light) diminishes the sensitivity of localization to nonlinear effects at this detuning.

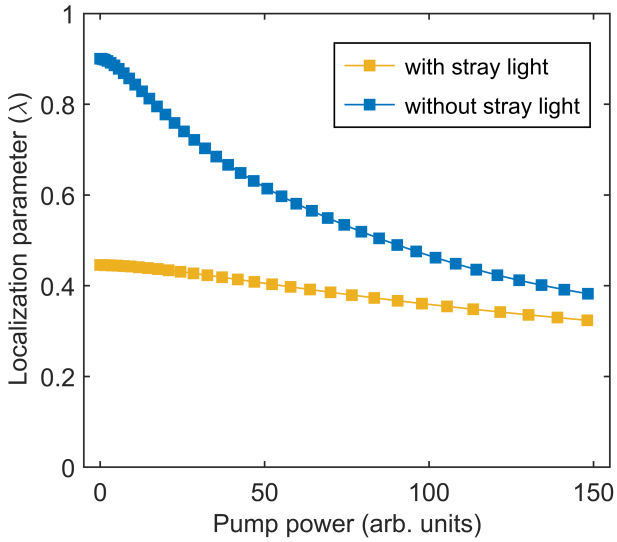

FIG. 8. Localization parameter λ as a function of pump power with and without stray light.

[1] A. Muñoz de las Heras, A. Amo, and A. González-Tudela, Nonlinearity-enabled localization in driven-dissipative photonic lattices, Phys. Rev. A **109**, 063523 (2024).